Short Paper

Simulation, Microfabrication, and Control of a Microheater Array

C. Zheng, G. P. S. Balasubramanian, Y. Tan, A. M. Maniatty, R. Hull, and J. T. Wen

***Abstract*—This paper describes the simulation, fabrication, and feedback control of a microheater array designed for the implementation of real-time control during thermal evolution of microstructure. The ten-channel heating array was designed through finite element simulation and microfabricated to be compatible with *in situ* imaging in a scanning electron microscope. Control algorithms are implemented that demonstrate cooperative control of the temperature (using calibrated Ti heater line resistances as a proxy) across the set of channels in the array. The goal of this system is to be able to generate controlled thermal, and thus microstructural, and property distribution during processing of polycrystalline materials.**

***Index Terms*—Finite element method (FEM), material processing, microstructure control, thermal control.**

I. Introduction

The control of local microstructure, e.g., grain size distributions, and thus properties, is an important goal of materials processing. For example, several critical mechanical phenomena such as yield, fatigue, and creep are known to depend sensitively upon grain size and distributions in polycrystalline materials. While a great deal is known about structure-property-processing relations in many systems, the realization of controlled variations in microstructure and properties is much more complex. Methods do not currently exist to dynamically intervene during materials processing to achieve a desired target microstructure. In addition, process control, while implemented in many materials processing and manufacturing applications, is generally targeted to maintaining a desired set of fixed states or programmed transitions of processing parameters, rather than actively adapting the processing conditions. In this paper, we seek to implement hardware and control solutions that enable dynamical adjustment of thermal processing conditions so that desired microstructures can be realized. Our objective is to create a temperature programmable microheater array that can be operated inside a scanning electron microscope (SEM), such that we are able to control temperature distribution across a macroscopic sample and observe microstructure evolution in real time.

There have been several papers in the literature addressing techniques for microscale temperature manipulation, especially for applications in microfluidic devices, e.g., [1]. A thin layer of either platinum or titanium is typically used both as heater and temperature sensor [2]. The objectives of these devices are two-fold: either to reach a uniform temperature field or a certain temperature gradient. In [3], microheater arrays are shaped to compensate boundary effects and hence realize better uniformity. Shape optimization of the resistive heaters is also used in [4] to achieve a linear temperature profile. In [5], a device with four microheaters placed along a square is designed to generate a temperature gradient for thermal-capillary actuation of microdroplets. A locally-addressable microheater array is described in [6] to generate high-resolution surface temperature fields with numerical heat transfer calculations performed to study the heating performance, e.g., temperature resolution and response time, etc. These methods have been developed for specific applications; some aim at solely a constant profile, some use only single bulk temperature sensing as feedback and some try to achieve large gradients but not necessarily feedback control for accurate local temperature regulation [1]. In our case, multiple local temperature sensing and feedback are both needed to achieve the desired temperature distribution for microstructure control, in contrast to only bulk temperature feedback in the past.

In this paper, a heater array similar to that reported in [6] and [7] is designed and fabricated. Our goal is to develop a control algorithm to regulate the temperature distribution in the heater array. The voltage across each titanium heater—and the current passing through each line and the corresponding Joule heating—is independently controlled to achieve different target temperature profiles. We use calibrated resistances of the heaters themselves as a proxy for the local temperature measurement. Both decentralized and consensus-based resistance feedback control are applied to demonstrate spatial temperature control. The finite element method (FEM) modeling, as described in [8], is used to guide the heater design as well as the controller design. In the physical experiment, the heater array is used to achieve uniform resistance for a sample with initially nonuniform resistance.

II. Design, Simulation, And Fabrication of Heater Arrays

We have designed a microheater array for temperature control across a thin film. A cross-sectional view of the active heater structure is shown in Fig. 1. This device consists of ten individually electrically addressable Ti lines fabricated within a SiO_2 matrix, on a Si substrate. To obtain significant microstructure evolution in the target Cu film, the overall array is designed to be externally heated to 200–300°C,

Manuscript received January 6, 2016; revised April 28, 2016 and September 6, 2016; accepted October 13, 2016. Date of publication January 9, 2017; date of current version August 14, 2017. Recommended by Technical Editor Q. Zou. This work was supported in part by the National Science Foundation as part of the Designing Materials to Revolutionize and Engineer our Future (DMREF) Program under Grant NSF-CMMI 1334283, and in part by the Center for Automation Technologies and Systems, Rensselaer Polytechnic Institute, under a block grant from the New York State NYSTAR Contract under Grant C130145. *(C. Zheng and G.P.S. Balasubramanian contributed equally to this work.)*

C. Zheng, Y. Tan, and A. M. Maniatty are with the Department of Mechanical, Aerospace, and Nuclear Engineering, Rensselaer Polytechnic Institute, Troy, NY 12180 USA (e-mail: zhengc2@rpi.edu; tany3@rpi.edu; maniaa@rpi.edu).

G. P. S. Balasubramanian and R. Hull are with the Department of Materials Science and Engineering, Rensselaer Polytechnic Institute, Troy, NY 12180 USA (e-mail: prabhu.ganapathi@gmail.com; hullr2@rpi.edu).

J. T. Wen is with the Department of Industrial and Systems Engineering, and also with the Department of Electrical, Computer, and Systems Engineering, Rensselaer Polytechnic Institute, Troy, NY 12180 USA (e-mail: wenj@rpi.edu).

Color versions of one or more of the figures in this paper are available online at http://ieeexplore.ieee.org.

Digital Object Identifier 10.1109/TMECH.2017.2650682

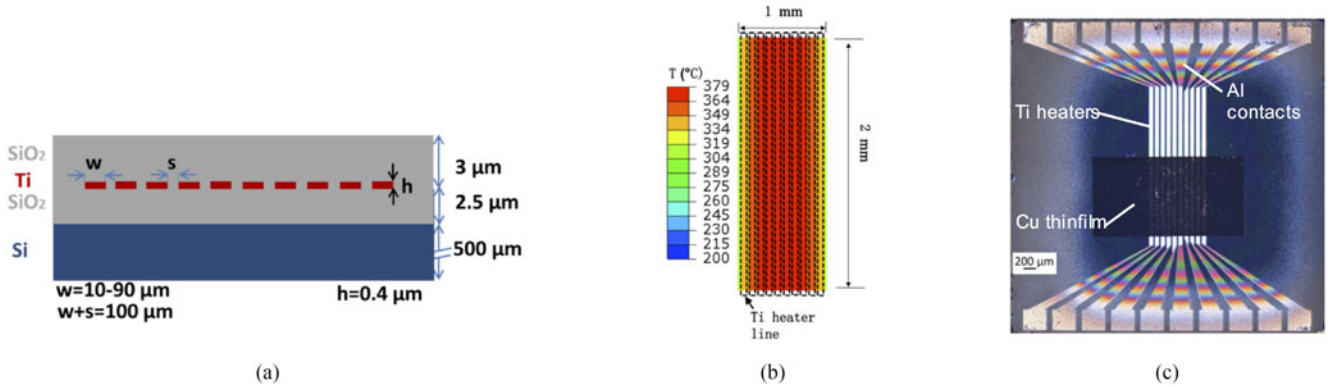

Fig. 1. (a) Schematic cross section of heater array. (b) Finite element calculation of temperature distribution across surface of upper SiO_2 layer with 240 mA passing through each of 70-μm wide heater lines and substrate maintained at 200°C, Ti resistivity $= 1.3 \times 10^{-6}\ \Omega \cdot m^{-1}$. The dotted black boxes show the positions of the Ti heater lines. (c) Optical image of an example completed heater array. The dark rectangular feature is a Cu film that is nominally 4-μm thick. Panel (c) is adapted from [9] with permission. Copyright: Materials Research Society 2016.

with resistive heating of the Ti heater lines providing an additional range of 0–100°C at the SiO_2 surface where the polycrystalline Cu metal is deposited. The current density in the Ti lines should be kept below about 10^6 A · cm^{-2} to avoid rapid failure due to electromigration [10]–[12]. We restrict the entire heater array structure to within an area 1 cm^2 in size and the active heater area within about 1 mm^2. These dimensions are designed to be consistent with an SEM heating stage, and the available field of view during SEM imaging, respectively. The restriction of the active area of the heating array translates into a pitch of 100 μm between adjacent heater lines.

As an initial validation of the heater array design, a three-dimensional FEM model is used to predict surface temperatures as a function of Ti line dimensions (width and thickness) and current through the Ti lines. Fig. 1(b) shows the results with Ti wires of 70-μm width and 400-nm thickness with a current (density) of 240 mA (8.5×10^5 A · cm^{-2}) through each line and the underlying substrate held at 200°C. Radiation on the top SiO_2 surface is calculated for an emissivity of 0.9 and ambient temperature of 25°C. The mesh size in this simulation is tested to be sufficiently fine to reach mesh convergence. It can be seen in Fig. 1(b) that the surface temperature at the top of the SiO_2 layer reaches almost 380°C, even with a fixed resistivity close to our measured room temperature resistivity $\approx 1.3 \times 10^{-6}\ \Omega \cdot m^{-1}$ rather than the higher values germane to higher temperatures. FEM model also predicts that thermal equilibrium is reached in 10 ms, which is much faster than the control step (5 s) and time constant of microstructure evolution (minutes to hours) for the relevant temperature range in Cu films.

An optical image of a fabricated heating array (with a Cu film deposited onto it using a shadow mask) is shown in Fig. 1(c). Fabrication of these heating arrays consists of the following procedure: A 2″ Si(100) wafer is first rinsed in water and then plasma cleaned. Following the O_2 plasma cleaning a 2.5 μm SiO_2 layer is deposited on a 2″ Si(100) wafer at 300°C, by plasma enhanced chemical vapor deposition. Next, a 400-nm Ti film is deposited by electron beam evaporation from a Ti source. Photoresist is then spun onto the surface of the Ti film, patterned using standard contact optical lithography techniques and used as a mask for etching the Ti layer using a buffered oxide etch. A second similar set of lithographic processes is performed to create Al contact lines to each of the Ti heater lines. Finally, the top 3 μm SiO_2 layer is deposited. Note that these thicknesses are nominal and will vary somewhat from chip to chip and wafer to wafer. The entire array is then extracted from the wafer and bonded to a standard chip carrier. Gold wire bonds are used to connect each Al contact pad to the corresponding contact on the chip carrier (i.e., 40 individual bonds in total, two at each end of each line). Note that for the experimental results reported in this paper, we use a heater array without a Cu film deposited.

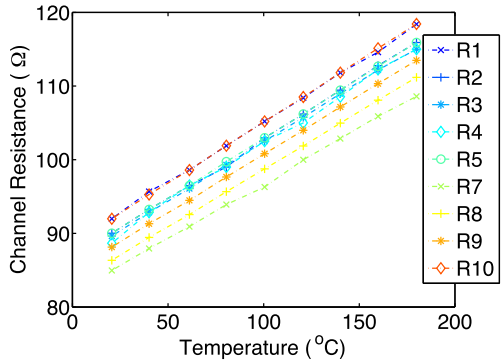

Fig. 2. Measured heater resistance versus top surface temperature. The measurements for the 6th resistance line, R6, are missing, as it was not functioning.

We use the measured (and controlled) resistances of the individual Ti lines as a proxy for the local temperature on top surface. This requires the calibration of the resistances of the Ti lines as a function of temperature. The relationship between measured channel resistances and top surface temperature for a heater array without a Cu film deposited is shown in Fig. 2. In our device, one of the heating line is defective (channel 6), so results in this paper are based on nine active heaters though ten are physically present on the device.

Resistance for each 90-μm wide Ti line (and thus 10 μm spacing between the lines) is measured in a Keithley probe station. The structure is heated incrementally from approximately 20 to 200°C, with no heating currents flowing through the lines for these calibration measurements. At different temperatures, resistances of the nine functioning heater lines are measured using contact probes and a multimeter. The contact resistances, obtained through separate experiments, are estimated to be under 1 Ω.

III. Control Problem Formulation

The ultimate goal of this research is to control the grain growth and microstructure of the polycrystalline metal layer deposited on the heater array through Joule heating from the heater array. This paper represents an intermediate step toward that goal: Control the lateral

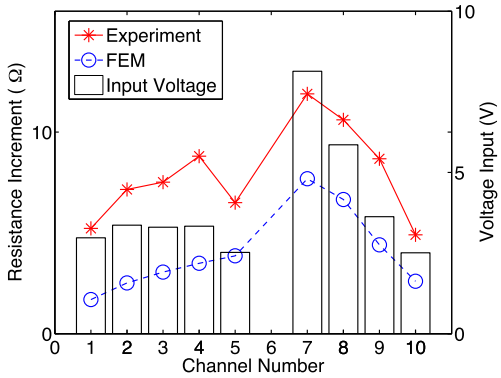

Fig. 3. Model and experiment temperature distribution comparison. Temperature field is interpreted as nine channels' resistance increments. The same voltage input as plotted as bars are used to energize the model and experimental structure. The controlled resistances are the same for all nine channels.

temperature distributions of the heater array by actively adjusting the voltages across the resistances of the heater lines.

A simplified 2-D FEM model described by [8] is used to guide the control design. Due to the dependence of material properties on the temperature distribution, the FEM model is nonlinear and is solved using the standard Newton–Ralphson method at each time step. With a constant input current u, the steady-state average temperature in the ten output zones are extracted from the FEM model and substituted into temperature–resistance mapping in Fig. 2 to yield the output vector y. The relationship between a constant input voltage vector u and the corresponding measured resistance vector y (used as a proxy for temperature) is then given by a static nonlinear map

$$y = F(u). \tag{1}$$

The primary control objective is output regulation, i.e., finding the input u to achieve the desired output resistance distribution y_d despite the uncertainty in F. A secondary objective is to minimize the transient variances in $y_d - y$ to avoid undesirable transient spatial temperature gradient. Note that the input/output mapping F is based on the FEM solution and, therefore, does not have an analytical expression. Furthermore, F is not exact, as indicated by the discrepancy in a sample comparison between model and experimental outputs in Fig. 3. However, the spatial distribution of the resistance increment has the same trend as the experiment. We will, therefore, use coarse properties, rather than the exact values, of F, and the measurement of the resistance vector y for the controller design.

IV. Feedback Controller Design

Let y_d be the specified desired output and u_d the corresponding input, i.e., $y_d = F(u_d)$. Directly solving for u_d is not possible, as F only approximates the physical reality. We propose using integral control based on the feedback of the resistance measurement y (shown in Fig. 4)

$$u_{k+1} = u_k - K_c(y_k - y_d) \tag{2}$$

where k is the discrete iteration of the feedback control and K_c is the integral feedback gain matrix. Proportional feedback control, $u_k = -K_p(y_k - y_d)$, may also be used but the feedback gain will be limited due to sampling and stability will be sensitive to time delays in the feedback loop. Substituting the input/output relationship for y_k and y_d

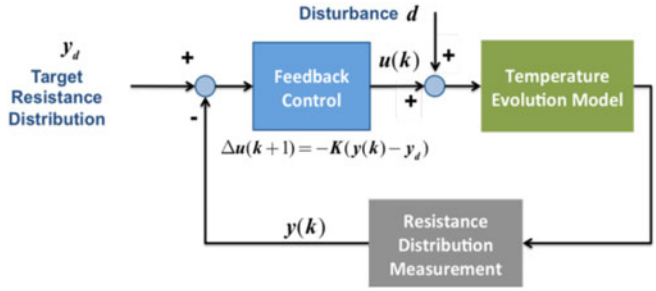

Fig. 4. Integral resistance feedback control regulates input voltage to achieve the desired resistance distribution.

in (2), we have

$$u_{k+1} = u_k - K_c(F(u_k) - F(u_d)). \tag{3}$$

Apply the mean value theorem [13] to $F(u_k) - F(u_d)$ and subtracting u_d on both sides, we have

$$(u_{k+1} - u_d) = (u_k - u_d) - K_c \nabla_u F(\xi_k)(u_k - u_d) \tag{4}$$

where ξ_k is some value on the line segment between u_k and u_d. Each input voltage (element of u) is limited to be in $[u_{\min}, u_{\max}]$. Denote this feasible region for u as $\mathcal{U}$. From the FEM model, we have numerically determined that $\nabla F(u)$ is positive and bounded for each $u \in \mathcal{U}$:

$$\frac{1}{2}\lambda_{\min}\left(\nabla F(u) + \nabla F(u)^T\right) = \gamma_u > 0 \tag{5}$$

$$\|\nabla F(u)\| \le \beta_u \tag{6}$$

where $\lambda_{\min}$ is the minimum eigenvalue and $\|\cdot\|$ denotes the induced 2-norm, β_u is the maximum singular value. The positivity property follows from the fact that the temperature, and resistance, measurements are collocated with the heaters and therefore change in the same direction as the input voltage. As shown in Appendix A, a sufficient condition for stability is that K_c is positive definite and satisfies

$$\|K_c\| < 2 \inf_{u \in \mathcal{U}} \frac{\gamma_u}{\beta_u^2}. \tag{7}$$

Choosing K_c to satisfy (7) assures the primary control objective of achieving the desired output at the steady state, i.e., $u_k \to u_d$ and hence $y_k \to y_d$ as $k \to \infty$. The secondary control objective is to keep the relative resistance distribution, differences between entries in y, small in the transient phase. To achieve both objectives, we choose K_c as the sum of two gains

$$K_c = K_{\text{diag}} + L \tag{8}$$

where K_{diag} is a positive definite matrix ensuring convergence of y to y_d, and an additional gain L is to reduce the transient spread of the entries in y. The gain K_{diag} may be chosen as a diagonal matrix for decentralized feedback, with each entry regulating the convergence rate of the corresponding input/output channel. The choice of L is motivated by network consensus control [14] where the differences between different agents are used in the feedback to enforce agreement. Treating each heater as a node, we form an graph as shown in Fig. 5 that connects every node with their four adjacent neighbors. For n nodes, this results in $\ell = 4n - 10$ links in the graph. Let D be the $\ell \times n$ graph incidence matrix, where $D_{ij} = 1$ if ith link points into the jth node, $D_{ij} = -1$ if ith link points out from the jth node, $D_{ij} = 0$, if ith link is not connected to the jth node. The weighting matrix W is diagonal with W_{ii} specifying the strength of connection of the ith link. We choose the gain L as the weighted Laplacian, $L = D^T W D$, which penalizes the difference between connected nodes and, thus,

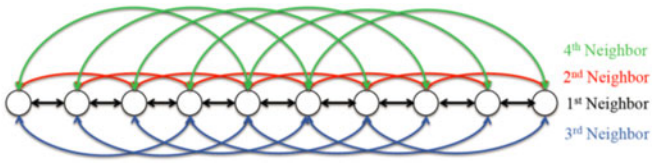

Fig. 5. Graph structure corresponding to the consensus feedback control. Note that in the physical experiment, channel 6 was defective and was, therefore, removed from the graph in the implementation. Adapted from [8] with permission. Copyright: IEEE 2016.

constrains the spread of y during the transient. Note that since L is only positive semidefinite but not positive definite, it cannot be used as K_c alone (K_c is required to be positive definite). Without K_{diag}, y_k would likely not converge to y_d. In addition to the stability condition (7), K_{diag} and W are tuned to achieve performance in terms of the speed of convergence and transient spatial gradient of y (variance of elements in y_k at each k). Gain selection involves the choice of two values: the scaling of $K_{\text{diag}} + L$ to ensure the stability condition is satisfied, and the relative weighting between K_{diag} and L for the tradeoff between the rate of convergence and variance of y_k. Since the overall gain scaling is determined by (7) and the desired robustness margin, we just need to tune the relative weighting of the two gains. This parameter is manually selected based first on the response in the nonlinear FEM simulation. It is then further adjusted based on the physical experiment (increase to speed up the response and decrease to avoid saturation).

V. Experimental Result

We have implemented the integral feedback controller (2) experimentally on our heater array. The goal is to achieve spatially uniform resistances by adjusting the voltages across heater array elements. The sample is initially under uniform temperature. Due to the different resistance-to-temperature curves as shown in Fig. 2, the initial spatial resistances are nonuniform. Conversely, under uniform resistances, the spatial temperature is nonuniform. Using data acquisition devices from National Instruments (NI USB 6218, NI 9264), a LabVIEW script is developed to provide the resistance-based temperature control. In the ith channel, the heater is serially connected to a small resistor of approximately $R_{s,i} \sim 10\,\Omega$, as shown in the circuit diagram (see Fig. 6). Voltages across the current-sensing resistor $v_{s,i}$ and the combined heater and current-sensing resistor u_i are measured with respect to a common ground. The resistance of the heater i is then calculated as

$$y_i = \left(\frac{u_i}{v_{s,i}} - 1\right) R_{s,i}. \tag{9}$$

Note that resistances of the wires and contacts affect this calculation, but their values are much smaller and, therefore, have a relatively minor effect. Resistances y_i are measured every one second and the control input u_i is updated every five seconds. The control implementation involves several constraints.

1) A minimum current is needed for resistance measurement. Therefore, a lower bound of $u_{\min} = 2\,\text{V}$ is needed for u_i.
2) An upper bound, $u_{\max} = 12\,\text{V}$, is imposed on u_i to avoid excessive current, which may cause electromigration failure and/or melting.
3) To protect the heater array from large transient thermal gradients and possible failure, a maximum increment on the voltage update of 0.5 V per control step is imposed. This is implemented as a saturation function for each u_i. Though saturation does not affect local stability, global asymptotic stability is no longer guaranteed in general.

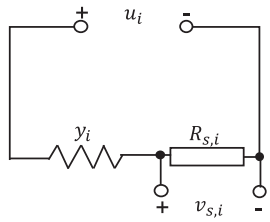

Fig. 6. Circuit diagram for heater resistance measurement.

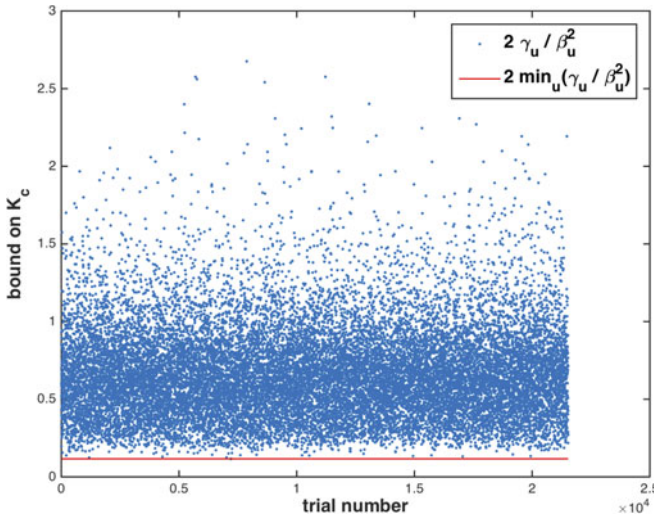

Fig. 7. Bounds from (7) based on random samples of $u \in \mathcal{U}$.

Based on the FEM model, we randomly sampled over 10 000 $u \in \mathcal{U}$ to obtain the bound in (7) (bounds from all samples are shown in Fig. 7)

$$2 \inf_{u \in \mathcal{U}} \frac{\gamma_u}{\beta_u^2} = 0.12\,\text{V}/\Omega. \tag{10}$$

The decentralized gain K_{diag} is chosen to be 0.02 in all diagonal entries. Since there are only nine working heater channels (channel 6 was defective), D is 26×9 and W is 26×26. The diagonal entries in W are set to 0.015 for the first neighbors, 0.01 for the second neighbors, 0.005 for the third and fourth neighbors. The feedback gain $K_c = K_{\text{diag}} + D^T W D$ is norm bounded by 0.11, which is slightly below the upper bound 0.12 in (10). Hence, we are assured of the closed-loop stability.

Experimental data from an array of ten 90 μm wide Ti lines (with nine functioning) without a Cu film deposited are shown in Fig. 8. Given the pitch of the line array, 100 μm, this means the temperature fields of the array of lines are strongly interacting, as their spacing is only 10 μm. Thus, the resistance/temperature of one line will strongly affect the resistance/temperature of adjacent lines as it heats the surrounding material, including the adjacent lines. This interdependence and the different thermal boundary conditions for the lines result in a strong need for the cooperative rather than decentralized control algorithm.

The initial resistances of the Ti heater lines (with the minimum voltage of 2 V on each channel applied for measurements) vary between 82 and 92 Ω. Through feedback control, regulation of resistances to a uniform value is effective using both $L = 0$ and $L \neq 0$, over time constants of a few minutes as illustrated in Fig. 8(a) and (c). Fig. 8(b) and (d) illustrates the corresponding controlled evolution of the voltage inputs to each channel. With fully decentralized feedback, $L = 0$, shown in Fig. 8(b), several channels initially overshoot because channels close to them are still being heated. Augmenting the decentralized feedback by consensus feedback, $L \neq 0$, shown in Fig. 8(d), results in

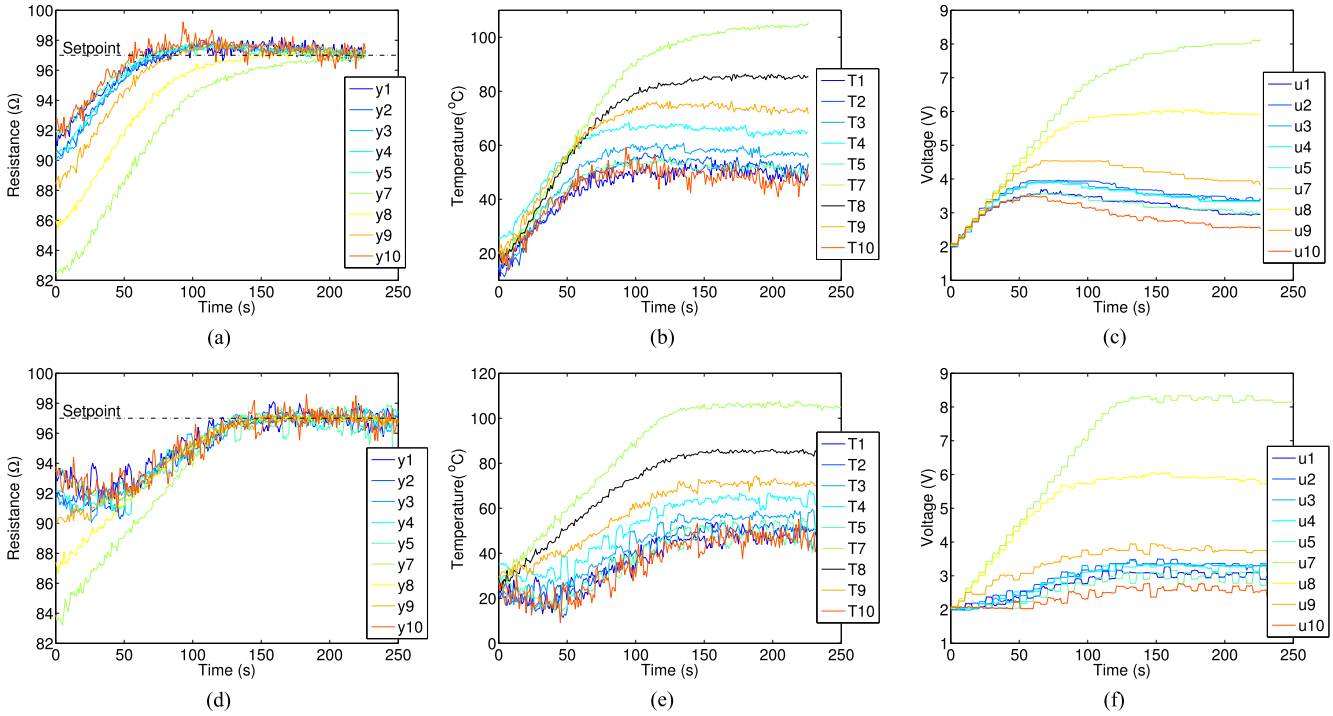

Fig. 8. Experimental resistance output and voltage input of individual heater lines. (a)–(c): Decentralized feedback ($L = 0$). (d)–(f): Cooperative feedback ($L = D^T W D$). The objective is to regulate channel resistances uniformly to the set point. Resistances are measured every one second and control input is updated every five seconds. Temperature is inferred from resistance–temperature relationship in Fig. 2. Channel 6 was defective in the experiment. The steady-state resistances are as same as that in Fig. 3. Panels (a) and (d) are adapted from [9] with permission. Copyright: Materials Research Society 2016.

TABLE I
PERFORMANCE COMPARISON BETWEEN $K_c = K_{\text{DIAG}}$ AND $K_c = K_{\text{DIAG}} + D^T W D$ IN TERMS THE SETTLING TIME OF EACH CHANNEL AND ℓ_2 AND ℓ_∞ NORMS OF THE VARIANCE OF y_k, $\text{V}(y_k)$

Gain	10% Settling time (s)	$\|\text{V}(y_k)\|_\infty$	$\|\text{V}(y_k)\|_2$
Decentralized	(189.0, 123.1, 60.3, 59.4, 134.0, 126.8, 97.3, 68.0, 175.1)	10.5	679.5
Cooperative	(124.1, 124.9, 124.3, 125.5, 138.9, 115.3, 115.1, 122.8, 127.0)	11.0	261.5

each channel converging to the desired resistance more rapidly. Those channels with initially higher resistance would wait for other channels. Once consensus is reached, they converge together to the set point. The numerical comparison is shown in Table I. Under the decentralized feedback alone, the settling times are widely different, and the cumulative variance of y_k is large as a result. Under the cooperative feedback, the settling times are close to each other and the cumulative variance of y_k is reduced almost by a factor of 3. The local response of the closed loop system is determined by the nine-input/nine-output closed-loop linearized system (from the desired resistance to actual resistance) about the set point. Since this is a multivariable system, the speed of the response is determined by the linear combination of nine modes (corresponding to the poles of the system), as well as the initial and target resistance values. For the cases corresponding to the experiment, the time constants of the nine output resistance measurements range from 30 to 60 s for the decentralized feedback gain and 21 to 68 s for the cooperative feedback gain. For the cooperative feedback case, the response speed of line 7 is significantly increased (with time constant dropping from 55 to 27 s) as its initial value is farthest away from the set point.

VI. CONCLUSION

We have demonstrated the ability to create, control, and implement programmable temperature distributions (through the proxy of the resistance of the individual heater lines) in a microheater array that has been fabricated to be compatible with *in situ* real-time observations in an SEM. This has been achieved through integration of microfabrication processing, finite element modeling, and feedback control algorithms. The ability to demonstrate a desired resistance/temperature profile in a highly thermally interactive regime (90-μm wide heater strips separated by 10 μm), with convergence times of 2–3 min has been demonstrated.

APPENDIX A
STABILITY ANALYSIS

Define $e_{u_k} = u_k - u_d$ and $J_k = \nabla_u F(\xi_k)$. Multiply both sides of (4) by K_c^{-1}, we have

$$K_c^{-1} e_{u_{k+1}} = K_c^{-1} e_{u_k} - J_k e_{u_k}. \tag{11}$$

It follows:

$$\begin{aligned} e_{u_{k+1}}^T K_c^{-1} e_{u_{k+1}} &= e_{u_k}^T K_c^{-1} e_{u_k} - 2 e_{u_k}^T J_k e_{u_k} + e_{u_k}^T J_k^T K_c J_k e_{u_k} \\ &\le e_{u_k}^T K_c^{-1} e_{u_k} - (2\gamma_{\xi_k} - \beta_{\xi_k}^2 \|K_c\|) \|e_{u_k}\|^2. \end{aligned} \tag{12}$$

If K_c satisfies (7), then there exists a positive constant α such that

$$2\gamma_{\xi_k} - \beta_{\xi_k}^2 \|K_c\| \ge \alpha > 0.$$

Iterating on k, we have

$$e_{u_k}^T K_c^{-1} e_{u_k} \le e_{u_0}^T K_c^{-1} e_{u_0} - \alpha \sum_{i=0}^{k-1} \|e_{u_i}\|^2. \tag{13}$$

Letting $k \to \infty$, we have $\|e_{u_i}\|$ as an ℓ_2 sequence, which implies that $e_{u_i} \to 0$ as $i \to \infty$.

Acknowledgment

The authors would like to acknowledge extensive use of the Micro- and Nano-Scale Cleanroom Fabrication and Characterization Cores, administered by the Center for Materials, Devices, and Integrated Systems at Rensselaer Polytechnic Institute.

References

[1] V. Miralles, A. Huerre, F. Malloggi, and M.-C. Jullien, "A review of heating and temperature control in microfluidic systems: Techniques and applications," *Diagnostics*, vol. 3, no. 1, pp. 33–67, 2013.

[2] M. P. Dinca, M. Gheorghe, M. Aherne, and P. Galvin, "Fast and accurate temperature control of a PCR microsystem with a disposable reactor," *J. Micromech. Microeng.*, vol. 19, no. 6, 2009, Art. no. 065009.

[3] T.-M. Hsieh, C.-H. Luo, F.-C. Huang, J.-H. Wang, L.-J. Chien, and G.-B. Lee, "Enhancement of thermal uniformity for a microthermal cycler and its application for polymerase chain reaction," *Sens. Actuators B: Chem.*, vol. 130, no. 2, pp. 848–856, 2008.

[4] B. Selva, J. Marchalot, and M.-C. Jullien, "An optimized resistor pattern for temperature gradient control in microfluidics," *J. Micromech. Microeng.*, vol. 19, no. 6, 2009, Art. no. 065002.

[5] Z. Jiao, X. Huang, N.-T. Nguyen, and P. Abgrall, "Thermocapillary actuation of droplet in a planar microchannel," *Microfluidics Nanofluidics*, vol. 5, no. 2, pp. 205–214, 2008.

[6] A. A. Darhuber, S. M. Troian, and S. Wagner, "Generation of high-resolution surface temperature distributions," *J. Appl. Phys.*, vol. 91, no. 9, pp. 5686–5693, 2002.

[7] A. A. Darhuber, J. P. Valentino, S. M. Troian, and S. Wagner, "Thermocapillary actuation of droplets on chemically patterned surfaces by programmable microheater arrays," *J. Microelectromech. Syst.*, vol. 12, no. 6, pp. 873–879, 2003.

[8] C. Zheng, Y. Tan, J. T. Wen, and A. M. Maniatty, "Finite element model based temperature consensus control for material microstructure," in *Proc. Amer. Control Conf.*, Chicago, IL, USA, 2015, pp. 619–624.

[9] P. Balasubramanian *et al.*, "Substrates with programmable heater arrays for in-situ observation of microstructural evolution of polycrystalline films: Towards real time control of grain growth," *MRS Advances*, vol. 1, pp. 1947–1952, 2016.

[10] P. S. Balog and R. A. Secco, "High pressure and temperature behaviour of electrical resistivity of hcp metals Ti, Zr and Gd," *J. Phys.: Condens. Matter*, vol. 11, no. 5, pp. 1273–1287, 1999.

[11] E. A. Belskaya and E. Y. Kulyamina, "Electrical resistivity of titanium in the temperature range from 290 to 1800 K," *High Temp.*, vol. 45, no. 6, pp. 785–796, 2007.

[12] H. Zhang, G. Cargill, III, Y. Ge, A. Maniatty, and W. Liu, "Strain evolution in Al conductor lines during electromigration," *J. Appl. Phys.*, vol. 104, no. 12, 2008, Art. no. 123533.

[13] J. Hubbard and B. B. Hubbard, *Vector Calculus, Linear Algebra, and Differential Forms: A Unified Approach*, 4th ed. Beaverton, OR, USA: Matrix, 2009.

[14] B. Bamieh, M. R. Jovanović, P. Mitra, and S. Patterson, "Coherence in large-scale networks: Dimension-dependent limitations of local feedback," *IEEE Trans. Autom. Control*, vol. 57, no. 9, pp. 2235–2249, Sep. 2012.